

Physical-Layer Security for Frequency Diverse Array Based Directional Modulation in Fluctuating Two-Ray Fading Channels

Qian Cheng, *Student Member, IEEE*, Shilian Wang, *Member, IEEE*, Vincent Fusco, *Fellow, IEEE*,
Fanggang Wang, *Senior Member, IEEE*, Jiang Zhu, *Member, IEEE*, and Chao Gu

Abstract—The frequency diverse array (FDA) based directional modulation (DM) technology plays an important role in the implementation of the physical-layer security (PLS) transmission of 5G and beyond communication system. In order to meet the tremendous increase in mobile data traffic, a new design consuming less memory for the FDA-DM-based PLS transmission is urgently demanded. In this paper, an analytical symmetrical multi-carrier FDA model is proposed in three dimensions, namely, range, azimuth angle, and elevation angle, which differs from the conventional analytical approach with only range and azimuth angle considered. Then, a single-point (SP) artificial noise (AN) aided FDA-DM scheme is proposed, which reduces memory consumption of FDA-DM systems significantly compared with the conventional zero-forcing (ZF) and singular value decomposition (SVD) approaches. Moreover, the PLS performance of the proposed low-memory-consumption FDA-DM scheme is analyzed in fluctuating two-ray (FTR) fading channels for the first time, including bit error rate (BER), secrecy rate (SR), and secrecy outage probability (SOP). More importantly, the closed-form expressions for the lower bound of the average SR and the upper bound of the SOP are derived, respectively. The effectiveness of the analytical expressions is verified by numerical simulations. This work opens a way to lower the memory requirements for the DM-based PLS transmission of 5G and beyond communication system.

Index Terms—Directional modulation; frequency diverse array; fluctuating two-ray fading; physical-layer security; secrecy rate; secrecy outage probability.

I. INTRODUCTION

The work of Q. Cheng was supported by a scholarship from China Scholarship Council (CSC) under Grant 201803170247. The work of F. Wang was supported in part by the Beijing Natural Haidian Joint Fund under Grant L172020, in part by the National Natural Science Foundation under Grant 61571034 and Grant U1834210, in part by the Beijing Natural Science Foundation under Grant 4182051, in part by the State Key Laboratory of Rail Traffic Control and Safety under Grant RCS2019ZT011, and in part by the Major Projects of Beijing Municipal Science and Technology Commission under Grant Z181100003218010. (Corresponding Author: Shilian Wang; Vincent Fusco.)

Q. Cheng is with the College of Electronic Science, National University of Defense Technology, Changsha 410073, China, and also with the Institute of Electronics, Communications and Information Technology (ECIT), Queen's University Belfast, Belfast BT3 9DT, U.K. (e-mail: chengqian14a@nudt.edu.cn).

S. Wang and J. Zhu are with the College of Electronic Science, National University of Defense Technology, Changsha 410073, China (e-mail: wangsl@nudt.edu.cn, jiangzhu@nudt.edu.cn).

V. Fusco and C. Gu are with the Institute of Electronics, Communications and Information Technology (ECIT), Queen's University Belfast, Belfast BT3 9DT, U.K. (e-mail: v.fusco@ecit.qub.ac.uk, chao.gu@qub.ac.uk).

F. Wang is with the State Key Laboratory of Rail Traffic Control and Safety, Beijing Jiaotong University, Beijing 100044, China (e-mail: wangfg@bjtu.edu.cn).

PHYSICAL-LAYER security (PLS) is one of the most important aspects of 5G and beyond wireless communications [1]. Implementing the PLS transmission can result in considerable memory consumptions, which imposes stringent requirements on the 5G nodes or devices. In addition, the tremendously increasing mobile data traffic also requires considerable memory consumptions. Therefore, it is highly necessary to lower the memory consumption of the PLS transmission strategy for 5G and beyond communication system.

The directional modulation (DM) technology [2], which is capable of steering the standard baseband symbols along a desired direction while simultaneously distorting the received signals along other directions, has been regarded as a useful PLS transmission strategy for 5G millimeter-wave (mmWave) wireless communications [3][4]. Traditionally, DM technology is implemented using phased arrays (PA) [5], which only achieves one-dimension security in the direction while loses security if the eavesdropper is in the same direction as the legitimate receiver. Compared with the PA-based DM technology, the frequency diverse array (FDA), exhibiting an extra range-dimension dependence apart from angle [6][7], has been applied into DM implementations to realize two-dimension security in both range and angle.

Specifically, the FDA was first utilized in [8] to achieve range-angle dependent secure DM transmissions with fixed linear frequency increments. The work in [9] utilized the FDA with non-linear frequency increments to decouple range- and angle-dependent transmit beam patterns for DM transmissions. The FDAs with random and time-modulated frequency increments were exploited for secure DM transmissions in [10] and [11], respectively. FDA was also used in [12][13] to establish secure DM transmissions for proximal legitimate user and eavesdropper. In addition to the single-user FDA-DM schemes [8]-[13], multi-user FDA-DM schemes were also investigated intensively by means of the spread spectrum technology [14], optimization algorithms [15], singular value decomposition (SVD) [16], weighted-type fractional Fourier transform (WFRFT) [17], respectively.

In the DM transmission schemes, artificial noise (AN) plays an important role. Most of the AN-aided DM transmission schemes employ zero-forcing (ZF) method to design the orthogonal precoding matrix to remove the interference of AN for legitimate receivers [10], [12], [15], [18]-[20]. The SVD method provided another way to redesign the orthogonal precoding matrix [16]. These ZF or SVD-aided design

approaches, however, consume too much memory to store the designed orthogonal matrix and AN. It still remains a challenge to design a secure DM transmission scheme with low memory consumption for 5G and beyond communication system. Moreover, the afore mentioned DM-related works [8]-[20] only considered the line-of-sight (LoS) channels in free space. Regarding the FDA-DM transmission in multipath fading channels, the authors in [21] and [22][23] investigated the PLS performance of the FDA-DM communication system in Rayleigh and Nakagami- m fading channels, respectively.

However, on the one hand, the works in [21]-[23] about FDA-DM transmissions in fading channels utilized ZF-based AN method, which demand high memory requirements as well. On the other hand, these conventional fading models like Rayleigh, Rician and Nakagami- m fading cannot accurately fit the random small-scale fluctuations in real communication environments [24]. Recently, the fluctuating two-ray (FTR) fading model was proposed in [24][25], which can provide a better fit for small-scale fading measurements in mmWave communications. The authors in [26], [27] and [28] generalized the FTR fading model into arbitrary fading parameter case, cascaded case, and squared case, respectively. More recently, the secrecy rate (SR), secrecy outage probability (SOP) and symbol error rate (SER) of FTR fading channels were analyzed in [29], [30] and [31] without AN (NoAN), respectively. The power adaption algorithm and wireless-powered UAV relay communication in FTR fading channels were investigated in [32] and [33], respectively.

To the best of our knowledge, there is no specific work in the state-of-the-art that aims to reduce the memory consumption of the FDA-DM scheme for 5G and beyond communications and to analyze the PLS performance of the FDA-DM scheme in FTR fading channels. We are the first to make this effort by proposing a low-memory-consumption single-point (SP) AN-aided FDA-DM scheme for 5G and beyond communications, and analyzing its PLS performance in FTR fading channels for the first time. Overall, the main contributions of our work are as follows:

- 1) Different from the conventional analytical approach which only considers range and azimuth angle dimensions, an analytical model for the symmetrical multi-carrier FDA is proposed in three dimensions, i.e., range, azimuth angle and elevation angle.
- 2) Based on the proposed FDA model, a low-memory-consumption FDA-DM scheme is further proposed with the assistance of single-point AN, which significantly outperforms the conventional ZF method [10], [12], [15], [18]-[23] and the SVD method [16]. The proposed low-memory-consumption FDA-DM scheme provides an efficient strategy to lower the memory requirements for the PLS transmissions of 5G and beyond communications.
- 3) The bit error rate (BER), SR and SOP performances of the proposed FDA-DM scheme are analyzed in FTR fading channels for the first time. We also derive the closed-form expressions for the lower bound of average SR and the upper bound of SOP. Numerical experiments are conducted to compare the PLS performances of the proposed SP and the conventional ZF [10], [12], [15],

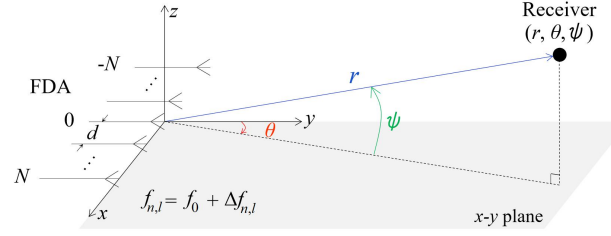


Fig. 1. The proposed FDA-DM scheme in FTR fading channels.

[18]-[23], SVD [16] and NoAN [29]-[31] methods.

The remainder of this paper is organized as follows. Section II proposes an analytical model of symmetrical multi-carrier FDA in three dimensions. A low-memory-consumption FDA-DM scheme is proposed in Section III with the assistance of single-point AN, where the comparison between the proposed SP method and the conventional ZF and SVD methods is also provided. Section IV analyzes the BER, average SR and SOP performances of the proposed FDA-DM scheme in FTR fading channels. Numerical results are conducted in Section V in order to verify the advantages of the proposed FDA-DM scheme. Finally, Section VI makes a conclusion for the whole paper and points out the future work.

Notations: In this paper, $i = \sqrt{-1}$ indicates imaginary unit. The operators $(\cdot)^T$ and $(\cdot)^H$ represent the transpose and the Hermitian transpose of a matrix. The set of complex numbers is denoted by \mathbb{C} . The notation $\mathbb{E}(\cdot)$ refers to the expectation of a random variable, while $\text{tr}(\cdot)$ represents the trace of a matrix. In addition, $\max\{\cdot\}$ and $|\cdot|$ refer to the maximum value of a set of real numbers and the modulus of a complex number, respectively. $\mathcal{N}(0, \sigma^2)$ and $\mathcal{CN}(0, \sigma^2)$ refer to the real and complex Gaussian distributions with zero mean and variance σ^2 , respectively. $\mathcal{U}[\cdot, \cdot]$ is the uniform distribution. Finally, the probability function is denoted by $\text{Pr}(\cdot)$.

II. FDA MODEL IN THREE DIMENSIONS

Most of the state-of-the-art analyzes the FDA only in two dimensions [6]-[17], namely, range and azimuth angle. In this paper, we take an extra dimension, elevation angle, into consideration and establish an analytical FDA model in three dimensions, i.e., range, azimuth angle, and elevation angle.

As shown in Fig. 1, the FDA consists of $2N + 1$ antenna elements with equal element spacing d , which is set as half wavelength of the central carrier. These elements are symmetrically and linearly arrayed on the x -axis with the central element located at the coordinate origin. For each element, there are L subcarriers to transmit. The radiated frequency of the l -th ($l = 0, \dots, L - 1$) subcarrier of the n -th ($n = -N, \dots, 0, \dots, N$) element is designed as

$$\begin{aligned} f_{n,l} &= f_0 + \Delta f_{n,l} \\ &= f_0 + \Delta f \ln(|n| + 1) \ln(l + 1) \end{aligned} \quad (1)$$

where f_0 is the central radiated frequency, Δf refers to a fixed frequency increment, and $\Delta f_{n,l} = \Delta f \ln(|n| + 1) \ln(l + 1)$ represents the frequency increment between the central frequency and the l -th subcarrier of the n -th element, which satisfies

$$|\Delta f_{n,l}| \ll f_0 \quad (2)$$

In order to derive the steering vector of the FDA, we consider that each element of the transmitter transmits sinusoidal signals with L subcarriers. The l -th subcarrier signal transmitted by the n -th element at time t can be expressed as

$$x_{n,l}(t) = e^{i2\pi f_{n,l}t} \quad (3)$$

Let r , θ and ψ represent the range, azimuth angle and elevation angle, respectively, as shown in Fig. 1. For an arbitrary receiver located at (r, θ, ψ) , the overall observed signal in the far field can be written as

$$y(r, \theta, \psi) = \sum_{n=-N}^N \sum_{l=0}^{L-1} x_{n,l} \left(t - \frac{r_n}{c} \right) \quad (4)$$

$$= \sum_{n=-N}^N \sum_{l=0}^{L-1} \exp \left\{ i2\pi f_{n,l} \left(t - \frac{r_n}{c} \right) \right\} \quad (5)$$

where c denotes light speed and r_n refers to the path length from the n -th element to the observation point. With the far field approximation, r_n can be calculated as

$$r_n \approx r - nd \sin \theta \cos \psi \quad (6)$$

Taking (1) and (6) into (5) yields

$$\begin{aligned} y(r, \theta, \psi) &\approx \sum_{n=-N}^N \sum_{l=0}^{L-1} \exp \left\{ i2\pi (f_0 + \Delta f_{n,l}) \left(t - \frac{r - nd \sin \theta \cos \psi}{c} \right) \right\} \\ &= \exp \left\{ i2\pi f_0 \left(t - \frac{r}{c} \right) \right\} \sum_{n=-N}^N \sum_{l=0}^{L-1} \exp \left\{ i2\pi \left[\Delta f_{n,l} \left(t - \frac{r}{c} \right) \right. \right. \\ &\quad \left. \left. + \frac{1}{c} f_0 nd \sin \theta \cos \psi + \frac{1}{c} \Delta f_{n,l} nd \sin \theta \cos \psi \right] \right\} \end{aligned} \quad (7)$$

The constraint in (2) implies that the last term in the summation, $\Delta f_{n,l} nd \sin \theta \cos \psi / c$, can be omitted, so (7) can be further approximated as

$$\begin{aligned} y(r, \theta, \psi) &\approx \exp \left\{ i2\pi f_0 \left(t - \frac{r}{c} \right) \right\} \\ &\cdot \sum_{n=-N}^N \sum_{l=0}^{L-1} \exp \left\{ i2\pi \left[\Delta f_{n,l} \left(t - \frac{r}{c} \right) + \frac{1}{c} f_0 nd \sin \theta \cos \psi \right] \right\} \end{aligned} \quad (8)$$

The terms inside the summation of (8) are decided by the geometry and the frequency-offset scheme of the FDA. Therefore, the sub-steering vector caused by the L subcarriers of the n -th antenna element can be written as [34]

$$\begin{aligned} \mathbf{a}_n(r, \theta, \psi) &= \left[e^{i2\pi (\Delta f_{n,0} (t - \frac{r}{c}) + \frac{1}{c} f_0 nd \sin \theta \cos \psi)} \dots \right. \\ &\quad e^{i2\pi (\Delta f_{n,L-1} (t - \frac{r}{c}) + \frac{1}{c} f_0 nd \sin \theta \cos \psi)} \dots \\ &\quad \left. e^{i2\pi (\Delta f_{n,L-1} (t - \frac{r}{c}) + \frac{1}{c} f_0 nd \sin \theta \cos \psi)} \right]^T \end{aligned} \quad (9)$$

which is an $L \times 1$ vector.

Therefore, the overall normalized steering vector of the symmetrical multi-carrier FDA can be calculated as

$$\begin{aligned} \mathbf{h}(r, \theta, \psi) &= \frac{1}{\sqrt{(2N+1)L}} \\ &\cdot \left[\mathbf{a}_{-N}^T(r, \theta, \psi) \dots \mathbf{a}_n^T(r, \theta, \psi) \dots \mathbf{a}_N^T(r, \theta, \psi) \right]^T \end{aligned} \quad (10)$$

III. LOW-MEMORY-CONSUMPTION FDA-DM SCHEME IN FTR FADING CHANNELS

We consider a multi-input single-output single-eavesdropper (MISOSE) wiretap channel model. In this model, a legitimate transmitter (Alice), equipped with a $(2N+1)$ -element symmetrical FDA with each element having L subcarriers, intends to deliver confidential information to a legitimate receiver (Bob), while an eavesdropper (Eve) at a different location tries to wiretap the confidential information. As analyzed in Section II, the central element of Alice's FDA is the coordinate origin, meanwhile Bob's and Eve's locations are assumed to be (r_B, θ_B, ψ_B) and (r_E, θ_E, ψ_E) , respectively. We also assume both Bob's and Eve's channels are in the FTR fading.

A. Alice's Transmit Signal

The transmit signal of Alice consists of two parts. The first is the normalized baseband modulation symbol $s \in \Omega$ and $\mathbb{E}(|s|^2) = 1$, where Ω is the alphabet of the baseband modulation symbols with the size of M . The second is the inserted single-point AN z , which follows a complex Gaussian distribution, i.e., $z \sim \mathcal{CN}(0, 1)$. To match the $(2N+1)L$ FDA subcarriers of Alice, the baseband symbol s and the inserted AN z should be precoded with a normalization vector \mathbf{p}_1 and an orthogonal vector \mathbf{p}_2 , respectively, which require

$$\mathbf{h}_B^H \mathbf{p}_1 = 1 \quad (11)$$

and

$$\mathbf{h}_B^H \mathbf{p}_2 = 0 \quad (12)$$

where $\mathbf{h}_B = \mathbf{h}(r_B, \theta_B, \psi_B)$ is the normalized steering vector at Bob's location.

Therefore, the transmitting signal vector which feeds Alice's $2N+1$ antenna elements can be expressed as

$$\mathbf{x} = \beta_1 \sqrt{P_s} \mathbf{p}_1 s + \alpha \beta_2 \sqrt{P_s} \mathbf{p}_2 z \quad (13)$$

where P_s is the total transmitting power; $\alpha = 1/\sqrt{\text{tr}(\mathbf{p}_2 \mathbf{p}_2^H)}$ is the power normalization factor for the inserted AN; β_1 and β_2 are power splitting factors for the baseband symbol and the inserted AN, respectively, which satisfy the following constraint,

$$\beta_1^2 + \beta_2^2 = 1 \quad (14)$$

For the design of \mathbf{p}_1 and \mathbf{p}_2 , we first review the ZF method [10], [12], [15], [18]-[23] and the SVD method [16] briefly, and then propose a low-memory-consumption SP method.

1) *ZF method*: The normalization vector is directly designed as the normalized steering vector at Bob's location, i.e., $\mathbf{p}_1^{\text{ZF}} = \mathbf{h}_B$. In addition, the orthogonal matrix of the ZF method is designed as $\mathbf{P}_2^{\text{ZF}} = \mathbf{I}_{(2N+1)L} - \mathbf{h}_B \mathbf{h}_B^H$, which is actually a matrix with the size of $(2N+1)L \times (2N+1)L$. In order to match the orthogonal matrix \mathbf{P}_2^{ZF} , the inserted AN of the ZF method should be randomly valued from $\mathbf{z}^{\text{ZF}} \in \mathbb{C}^{(2N+1)L \times 1}$.

2) *SVD method*: Similar to the ZF method, the normalization vector of the SVD method is also designed as $\mathbf{p}_1^{\text{SVD}} = \mathbf{h}_B$. But for the design of the orthogonal matrix, the SVD method first solves the SVD of \mathbf{h}_B^H , i.e., $\mathbf{h}_B^H = \mathbf{U} [\mathbf{D} \mathbf{0}] [\mathbf{V}_1 \mathbf{V}_0]^H$, from which a null space of \mathbf{h}_B^H can be obtained. Then, the orthogonal matrix $\mathbf{P}_2^{\text{SVD}}$ can be directly designed as $\mathbf{P}_2^{\text{SVD}} = \mathbf{V}_0$, which

TABLE I
COMPARISON FOR MEMORY REQUIREMENTS OF DIFFERENT FDA-DM METHODS

Items	ZF [10], [12], [15], [18]-[23]	SVD [16]	Proposed SP
Orthogonal matrix/vector	$\mathbf{P}_2^{\text{ZF}} = \mathbf{I}_{(2N+1)L} - \mathbf{h}_B \mathbf{h}_B^H$	$\mathbf{h}_B^H = \mathbf{U} [\mathbf{D} \ 0] [\mathbf{V}_1 \ \mathbf{V}_0]^H$, $\mathbf{P}_2^{\text{SVD}} = \mathbf{V}_0$	$\mathbf{p}_2^{\text{SP}} = \text{Any orthogonal vector of } \mathbf{h}_B^H$
Size of orthogonal matrix/vector	$(2N+1)L \times (2N+1)L$	$(2N+1)L \times 2N$	$(2N+1)L \times 1$
Artificial noise	$\mathbf{z}^{\text{ZF}} \in \mathbb{C}^{(2N+1)L \times 1}$	$\mathbf{z}^{\text{SVD}} \in \mathbb{C}^{2N \times 1}$	$z^{\text{SP}} \in \mathbb{C}$
Size of artificial noise	$(2N+1)L \times 1$	$2N \times 1$	1
Total size	$(2N+1)^2 L^2 + (2N+1)L$	$2N(2N+1)L + 2N$	$(2N+1)L + 1$
Memory complexity	$\mathcal{O}(N^2 L^2)$	$\mathcal{O}(N^2 L)$	$\mathcal{O}(NL)$

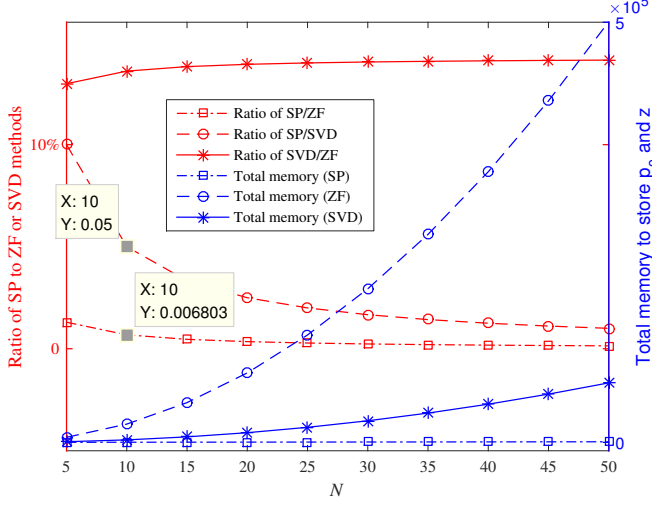


Fig. 2. Total memory required to store the orthogonal matrix/vector and the AN versus N ; and the ratio of the proposed SP method to ZF or SVD methods versus N . ($L = 7$)

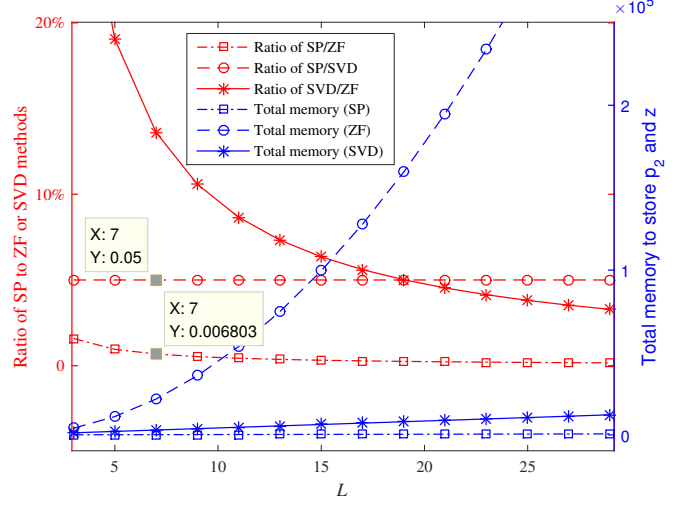


Fig. 3. Total memory required to store the orthogonal matrix/vector and the AN versus L ; and the ratio of the proposed SP method to ZF or SVD methods versus L . ($N = 10$)

is a matrix with the size of $(2N+1)L \times 2N$. Consequently, the inserted AN of the SVD method has to be changed as $\mathbf{z}^{\text{SVD}} \in \mathbb{C}^{2N \times 1}$ in order to match the orthogonal matrix $\mathbf{P}_2^{\text{SVD}}$.

3) *Proposed SP method*: The normalization vector in this paper is designed as $\mathbf{p}_1^{\text{SP}} = \mathbf{h}_B$ as well. Different from the ZF and SVD methods which insert an AN vector in the transmit signal, the proposed SP method only requires a single-point AN as shown in (13). Therefore, the orthogonal vector \mathbf{p}_2^{SP} can be designed as an arbitrary orthogonal vector of \mathbf{h}_B^H rather than a matrix. Comparatively, \mathbf{p}_2^{SP} can be an arbitrary column vector of \mathbf{P}_2^{ZF} or $\mathbf{P}_2^{\text{SVD}}$. In the following analysis, \mathbf{p}_2 specifically refers to the proposed \mathbf{p}_2^{SP} .

4) *Comparison for the ZF, SVD and SP methods*: In order to illustrate the advantage of the the proposed SP method, Table I compares these three different design methods in terms of memory consumption to store the orthogonal matrix/vector and the AN. From Table I, the proposed SP method reduces the memory complexity from $\mathcal{O}(N^2 L^2)$ and $\mathcal{O}(N^2 L)$ to $\mathcal{O}(NL)$, which significantly outperforms the ZF and SVD methods.

In addition, Fig. 2 and Fig. 3 depict the numerical results for the total memory required and the ratio of SP method to ZF or SVD methods versus N and L , respectively, which verify the excellent advantage of low memory consumption for the proposed SP method. For example, when $N = 10$ and $L = 7$,

the proposed SP method only requires approximately 0.68% total memory of the ZF method or 5% total memory of the SVD method. Fig. 4 and Fig. 5 further show the total memory consumptions and the corresponding ratios versus N and L , respectively, from which it demonstrates that the proposed SP method can save much more memory than the conventional ZF and SVD methods as well.

B. Bob's and Eve's Signals

After Alice transmits the signal, the received signal of Bob located at (r_B, θ_B, ψ_B) can be written as

$$y(r_B, \theta_B, \psi_B) = \epsilon_B \mathbf{h}_B^H \mathbf{x} + \xi_B \quad (15)$$

$$= \epsilon_B \beta_1 \sqrt{P_s} \mathbf{h}_B^H \mathbf{p}_1 s + \epsilon_B \alpha \beta_2 \sqrt{P_s} \mathbf{h}_B^H \mathbf{p}_2 z + \xi_B \quad (16)$$

$$= \epsilon_B \beta_1 \sqrt{P_s} s + \xi_B \quad (17)$$

where ξ_B is the complex additive white Gaussian noise (AWGN) with zero mean and variance δ_B^2 , i.e., $\xi_B \sim \mathcal{CN}(0, \delta_B^2)$. In addition, ϵ_B represents the FTR fading coefficient which is defined as [26]

$$\epsilon_B = \sqrt{\zeta_B} U_B e^{j\varphi_B} + \sqrt{\zeta_B} V_B e^{j\vartheta_B} + X_B + jY_B \quad (18)$$

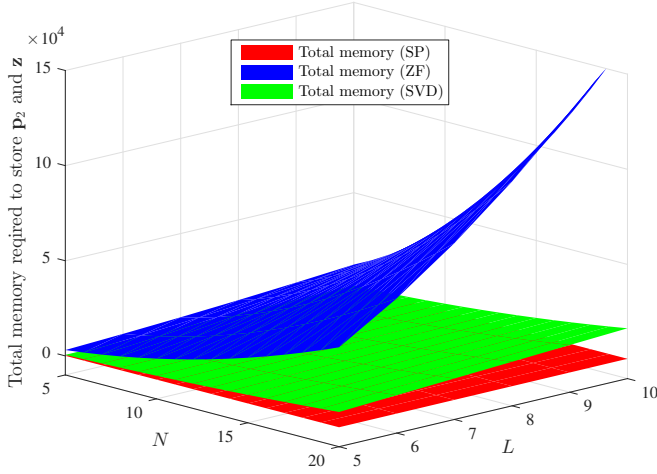


Fig. 4. Total memory required to store the orthogonal matrix/vector and the AN of the proposed SP method and the conventional ZF and SVD methods versus N and L .

where ζ_B is a Gamma distributed random variable with zero mean and probability density function given by

$$f_{\zeta_B}(\zeta_B) = \frac{m_B^{m_B} \zeta_B^{m_B-1}}{\Gamma(m_B)} e^{-m_B \zeta_B} \quad (19)$$

Moreover, U_B and V_B are constant amplitudes with specular components modulated by a Nakagami- m_B random variable. φ_B and ϑ_B are statistically independent and uniformly distributed random phases, i.e., $\varphi_B, \vartheta_B \sim \mathcal{U}[0, 2\pi)$. $X_B + \imath Y_B$ refers to the diffuse component with X_B and Y_B following a Gaussian distribution, i.e., $X_B, Y_B \sim \mathcal{N}(0, \sigma_B^2)$. The FTR fading parameters can be calculated by $K_B = \frac{U_B^2 + V_B^2}{2\sigma_B^2}$ and $\Delta_B = \frac{2U_B V_B}{U_B^2 + V_B^2}$. It can be observed from (17) that only the useful signal is left for Bob while the inserted AN has been removed, which guarantees the effective transmission between Alice and Bob.

Similarly, the received signal of Eve located at (r_E, θ_E, ψ_E) can be expressed as

$$y(r_E, \theta_E, \psi_E) = \epsilon_E \mathbf{h}_E^H \mathbf{x} + \xi_E \quad (20)$$

$$= \epsilon_E \beta_1 \sqrt{P_s} \mathbf{h}_E^H \mathbf{p}_1 s + \epsilon_E \alpha \beta_2 \sqrt{P_s} \mathbf{h}_E^H \mathbf{p}_2 z + \xi_E \quad (21)$$

$$= \underbrace{\epsilon_E \beta_1 \sqrt{P_s} \rho_1 s}_{\text{Distorted Signal}} + \underbrace{\epsilon_E \alpha \beta_2 \sqrt{P_s} \rho_2 z}_{\text{Artificial Noise}} + \underbrace{\xi_E}_{\text{AWGN}} \quad (22)$$

where $\xi_E \sim \mathcal{CN}(0, \delta_E^2)$ indicates the complex AWGN, $\mathbf{h}_E = \mathbf{h}(r_E, \theta_E, \psi_E)$ refers to Eve's normalized steering vector, $\rho_1 = \mathbf{h}_E^H \mathbf{p}_1$, and $\rho_2 = \mathbf{h}_E^H \mathbf{p}_2$. Additionally, the fading coefficient ϵ_E is defined as

$$\epsilon_E = \sqrt{\zeta_E} U_E e^{\imath \varphi_E} + \sqrt{\zeta_E} V_E e^{\imath \vartheta_E} + X_E + \imath Y_E \quad (23)$$

which undergoes the FTR fading with the parameters $(m_E, K_E, \Delta_E, \sigma_E^2)$.

It is worth noting that Eve's received signal in (22) consists of three items. The first is the useful signal distorted by ρ_1 and the second is the inserted AN. Both can be regarded as interference for Eve, thereby guaranteeing the PLS transmission between Alice and Bob.

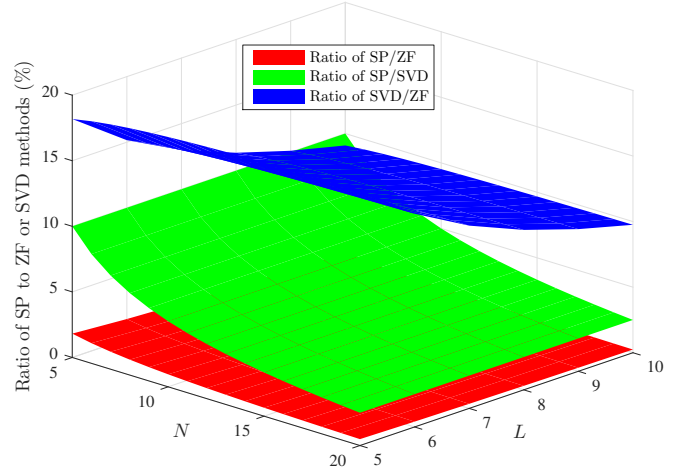


Fig. 5. The ratio of total memory of the SP method to that of the ZF or SVD methods versus N and L .

IV. PHYSICAL-LAYER SECURITY ANALYSIS

In this section, we will analyze the PLS performances of the proposed FDA-DM model including BER, SP and SOP, which are important metrics to measure the performances of DM transmission systems [35].

A. Bit Error Rate

To acquire the BER formula, we consider the case of no fading, which means $\epsilon_B = \epsilon_E = 1$. As a matter of fact, when the fading is considered, the derived BER formula can refer to [31] as long as the channel state information (CSI) [36][37] is fully estimated at Bob.

According to (17), the received signal of Bob is simply the summation of the useful signal and AWGN, and the average signal-to-noise ratio (SNR) of Bob can be written as

$$\gamma_B = \frac{\beta_1^2 P_s \mathbb{E}(|s|^2)}{\delta_B^2} \quad (24)$$

For an M -ary baseband modulation, the SNR per bit can be calculated by

$$\gamma_{\text{bit}} = \frac{\beta_1^2 P_s \mathbb{E}(|s|^2)}{\delta_B^2 \log_2 M} = \frac{\gamma_B}{\log_2 M} \quad (25)$$

Therefore, if PSK modulation is adapted, the BER formula for the proposed FDA-DM system can be calculated by [38]

$$\begin{aligned} P_e &\approx \frac{2}{\log_2 M} Q\left(\sqrt{2\gamma_{\text{bit}} \log_2 M} \sin \frac{\pi}{M}\right) \\ &= \frac{2}{\log_2 M} Q\left(\sqrt{2\gamma_B} \sin \frac{\pi}{M}\right) \end{aligned} \quad (26)$$

where $Q(u) = 1/\sqrt{2\pi} \int_u^\infty \exp\{-u^2/2\} du$ is the tail distribution function of the standard normal distribution.

B. Secrecy Rate

When the FTR fading is considered, we can rewrite the SNR of Bob as

$$\gamma_B = \frac{|\epsilon_B|^2 \beta_1^2 P_s \mathbb{E}(|s|^2)}{\delta_B^2} = \beta_1^2 \lambda_B \quad (27)$$

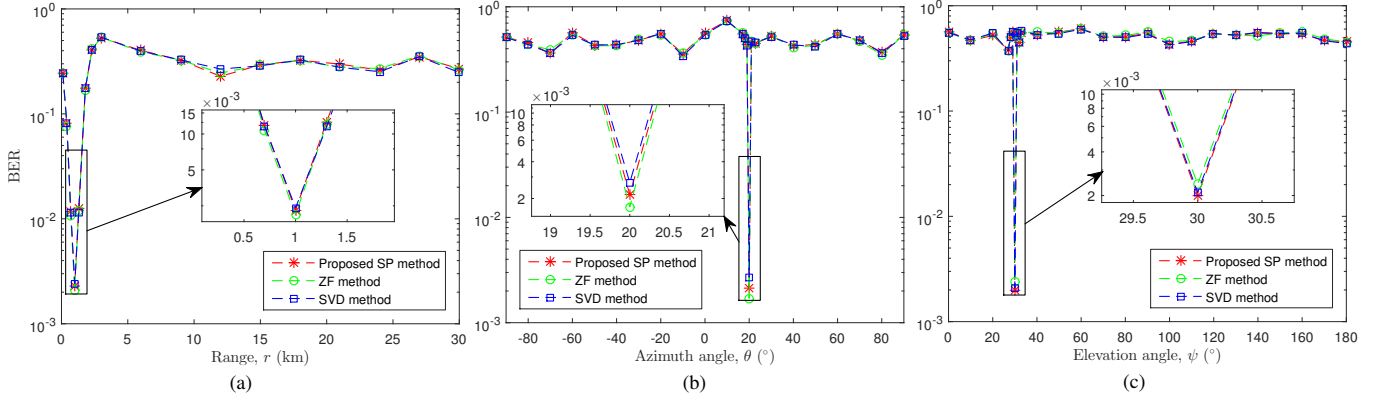


Fig. 6. BER versus (a) range r with $\theta = \theta_B = 20^\circ$ and $\psi = \psi_B = 30^\circ$, (b) azimuth angle θ with $r = r_B = 1$ km and $\psi = \psi_B = 30^\circ$, and (c) elevation angle ψ with $r = r_B = 1$ km and $\theta = \theta_B = 20^\circ$. ($f_0 = 30$ GHz, $\Delta f = 20$ kHz, $N = 10$, $L = 7$, $\beta_1 = 0.9$, QPSK, SNR = 10 dB)

where $\lambda_B = |\epsilon_B|^2 P_s \mathbb{E}(|s|^2) / \delta_B^2$ is Bob's SNR of the FTR fading channel without splitting AN, the average of which can be calculated by $\bar{\lambda}_B = \mathbb{E}(|\epsilon_B|^2) P_s \mathbb{E}(|s|^2) / \delta_B^2 = 2\sigma_B^2(1 + K_B)P_s / \delta_B^2$ [26].

According to (22), we can write the signal to inference-plus-noise (SINR) of Eve as

$$\gamma_E = \frac{|\epsilon_E|^2 \beta_1^2 |\rho_1|^2 P_s \mathbb{E}(|s|^2) / \delta_E^2}{|\epsilon_E|^2 \alpha^2 \beta_2^2 |\rho_2|^2 P_s \mathbb{E}(|z|^2) / \delta_E^2 + 1} \quad (28)$$

Let $\lambda_E = |\epsilon_E|^2 P_s \mathbb{E}(|s|^2) / \delta_E^2$, which indicates Eve's SNR of FTR fading channels without splitting AN, the average of which can be calculated by $\bar{\lambda}_E = \mathbb{E}(|\epsilon_E|^2) P_s \mathbb{E}(|s|^2) / \delta_E^2 = 2\sigma_E^2(1 + K_E)P_s / \delta_E^2$. Moreover, taking the assumption $\mathbb{E}(|s|^2) = \mathbb{E}(|z|^2) = 1$ into (28) yields

$$\gamma_E = \frac{\beta_1^2 |\rho_1|^2 \lambda_E}{\alpha^2 \beta_2^2 |\rho_2|^2 \lambda_E + 1} = \frac{\eta \lambda_E}{\mu \lambda_E + 1} \quad (29)$$

where $\eta = \beta_1^2 |\rho_1|^2$ and $\mu = \alpha^2 \beta_2^2 |\rho_2|^2$.

According to [26], the probability density function (PDF) and cumulative distribution function (CDF) of λ_i ($i \in \{B, E\}$) can be written as

$$f_{\lambda_i}(x) = \frac{m_i^{m_i}}{\Gamma(m_i)} \sum_{j_i=0}^{\infty} \frac{K_i^{j_i} d_{j_i}}{j_i! j_i!} \frac{x^{j_i}}{(2\sigma_i^2)^{j_i+1}} \exp\left(-\frac{x}{2\sigma_i^2}\right) \quad (30)$$

and

$$F_{\lambda_i}(x) = \frac{m_i^{m_i}}{\Gamma(m_i)} \sum_{j_i=0}^{\infty} \frac{K_i^{j_i} d_{j_i}}{j_i! j_i!} \Upsilon\left(j_i + 1, \frac{x}{2\sigma_i^2}\right) \quad (31)$$

where $j_i!$ denotes the factorial of the integer j_i ; $\Gamma(\cdot)$ and $\Upsilon(\cdot, \cdot)$ refer to the ordinary Gamma function [39, Eq. (8.310.1)] and the lower incomplete Gamma function [39, Eq. (8.350.1)], respectively. In addition, the term d_{j_i} in (30) and (31) is expressed as

$$\begin{aligned} d_{j_i} &\triangleq \sum_{k=0}^{j_i} \binom{j_i}{k} \left(\frac{\Delta_i}{2}\right)^k \sum_{l=0}^k \binom{k}{l} \Gamma(j_i + m_i + 2l - k) \\ &\cdot e^{i \frac{(2l-k)\pi}{2}} \left[(m_i + K_i)^2 - (K_i \Delta_i)^2 \right]^{-\frac{j_i+m_i}{2}} \\ &\cdot \mathcal{L}_{j_i+m_i-1}^{k-2l} \left(\frac{m_i + K_i}{\sqrt{(m_i + K_i)^2 - (K_i \Delta_i)^2}} \right) \end{aligned} \quad (32)$$

where $\binom{k}{l}$ denotes k chooses l , and $\mathcal{L}(\cdot)$ denotes the associated Legendre function of the first kind [39, Eq. (8.702)]. By observing (27), the PDF and CDF of γ_B can be easily calculated by (33) and (34), respectively

$$f_{\gamma_B}(x) = \frac{1}{\beta_1^2} f_{\lambda_B} \left(\frac{x}{\beta_1^2} \right) \quad (33)$$

$$F_{\gamma_B}(x) = F_{\lambda_B} \left(\frac{x}{\beta_1^2} \right) \quad (34)$$

Before deriving the PDF and CDF of γ_E , we first point out a fact that the lower and upper bounds of γ_E are 0 and $\tau = \eta/\mu$, respectively, which can be directly obtained by replacing $\lambda_E \rightarrow 0$ and $\lambda_E \rightarrow \infty$ into (29). Therefore, the CDF of γ_E can be acquired by

$$F_{\gamma_E}(x) = \Pr(\gamma_E \leq x) \quad (35)$$

$$= \Pr\left(\frac{\eta \lambda_E}{\mu \lambda_E + 1} \leq x\right) \quad (36)$$

$$= \Pr\left(\lambda_E \leq \frac{x}{\eta - \mu x}\right) \quad (37)$$

$$= \begin{cases} F_{\lambda_E} \left(\frac{x}{\eta - \mu x} \right), & 0 < x < \tau \\ 1, & x \geq \tau \end{cases} \quad (38)$$

Consequently, the PDF of γ_E can be calculated by

$$f_{\gamma_E}(x) = \frac{dF_{\gamma_E}(x)}{dx} \quad (39)$$

$$= \begin{cases} \frac{\eta}{(\eta - \mu x)^2} f_{\lambda_E} \left(\frac{x}{\eta - \mu x} \right), & 0 < x < \tau \\ 0, & x \geq \tau \end{cases} \quad (40)$$

Using the PDFs and CDFs of Bob's and Eve's SINRs, the instantaneous secrecy rate can be defined as

$$R_s(\gamma_B, \gamma_E) = \left[\log_2(1 + \gamma_B) - \log_2(1 + \gamma_E) \right]^+ \quad (41)$$

where $[\cdot]^+ = \max\{\cdot, 0\}$. If we further assume Bob's and Eve's channels experience independent fading, the average secrecy

rate can be calculated by [29]

$$\begin{aligned}\bar{R}_s(\gamma_B, \gamma_E) &= \int_0^\infty \int_0^\infty R_s(\gamma_B, \gamma_E) f(\gamma_B, \gamma_E) d\gamma_B d\gamma_E \\ &= \underbrace{\frac{1}{\ln 2} \int_0^\infty \ln(1 + \gamma_B) f_{\gamma_B}(\gamma_B) F_{\gamma_E}(\gamma_B) d\gamma_B}_{\mathcal{I}_1} \\ &\quad + \underbrace{\frac{1}{\ln 2} \int_0^\infty \ln(1 + \gamma_E) f_{\gamma_E}(\gamma_E) F_{\gamma_B}(\gamma_E) d\gamma_E}_{\mathcal{I}_2} \\ &\quad - \underbrace{\frac{1}{\ln 2} \int_0^\infty \ln(1 + \gamma_E) f_{\gamma_E}(\gamma_E) d\gamma_E}_{\mathcal{I}_3}\end{aligned}\quad (42)$$

where $f(\gamma_B, \gamma_E) = f_{\gamma_B}(\gamma_B) f_{\gamma_E}(\gamma_E)$ is the joint PDF of γ_B and γ_E .

Before deriving the secrecy rate, we define

$$\begin{aligned}\Psi(v_1, v_2, v_3, v_4, v_5, \tau) &= \int_0^\tau \ln^{v_1}(1+t) \frac{t^{v_2}}{(\tau-t)^{v_3}} \exp\left\{-v_4 t - \frac{v_5 t}{\tau-t}\right\} dt\end{aligned}\quad (43)$$

of which a special case is [29, Eq. (10)]

$$\mathcal{S}(u, v) = \Psi(1, u-1, 0, v, 0, \infty) \quad (44)$$

$$= \int_0^\infty \ln(1+t) t^{u-1} \exp\{-vt\} dt \quad (45)$$

$$= (u-1)! e^v \sum_{k=1}^u \frac{\Gamma(-u+k, v)}{v^k} \quad (46)$$

Then, the average secrecy rate can be obtained in Lemma 1 by substituting (33), (34), (38) and (40) into (42).

Lemma 1: The average secrecy rate of the proposed FDA-DM system in FTR fading is given by

$$\bar{R}_s(\gamma_B, \gamma_E) = \mathcal{I}_1 + \mathcal{I}_2 - \mathcal{I}_3 \quad (47)$$

where the expressions of \mathcal{I}_1 , \mathcal{I}_2 and \mathcal{I}_3 are listed in (48), (49) and (50), respectively. Moreover, the term χ in the expression of \mathcal{I}_1 is defined as

$$\begin{aligned}\chi &= \Psi(1, j_B, 0, \frac{1}{2\beta_1^2 \sigma_B^2}, 0, \tau) \\ &= \int_0^\tau \ln(1 + \gamma_B) \gamma_B^{j_B} \exp\left(-\frac{\gamma_B}{2\beta_1^2 \sigma_B^2}\right) d\gamma_B\end{aligned}\quad (51)$$

Proof: Please see Appendix A.

Asymptotically, when $\sigma_E^2 \rightarrow \infty$, a closed-form expression of the lower bound of the average secrecy rate is given in Lemma 2.

Lemma 2: When $\sigma_E^2 \rightarrow \infty$, the lower bound of the average secrecy rate of the proposed FDA-DM system in FTR fading can be written in the following closed-form expression,

$$\begin{aligned}\bar{R}_s^{\text{Low}}(\gamma_B, \gamma_E) &= \frac{m_B^{m_B}}{\ln 2 \Gamma(m_B)} \sum_{j_B=0}^{\infty} \frac{K_B^{j_B} d_{j_B}}{j_B! j_B! (2\beta_1^2 \sigma_B^2)^{j_B+1}} \\ &\quad \cdot [S(j_B + 1, \frac{1}{2\beta_1^2 \sigma_B^2}) - \chi] - \frac{\ln(1 + \tau)}{\ln 2} [1 - F_{\gamma_B}(\tau)]\end{aligned}\quad (52)$$

Proof: Please see Appendix B.

C. Secrecy Outage Probability

The secrecy outage probability is defined as the probability that the instantaneous secrecy rate R_s is less than a target secrecy rate R_0 , i.e.,

$$P_{\text{out}} = \Pr\{R_s(\gamma_B, \gamma_E) < R_0\} \quad (53)$$

$$= \Pr\left\{\log_2 \frac{1 + \gamma_B}{1 + \gamma_E} < R_0\right\} \quad (54)$$

Lemma 3: The SOP of the proposed FDA-DM system in FTR fading can be obtained by (55).

Proof: Please see Appendix C.

When $\sigma_E^2 \rightarrow \infty$, the upper bound of the SOP of the proposed FDA-DM system in FTR fading can be obtained by the following closed-form expression

$$P_{\text{out}}^{\text{Up}} = \Pr\left\{\log_2 \frac{1 + \gamma_B}{1 + \gamma_E} < R_0\right\} \Big|_{\sigma_E^2 \rightarrow \infty} \quad (56)$$

$$= \Pr\{\gamma_B < 2^{R_0}(1 + \tau) - 1\} \quad (57)$$

$$= F_{\gamma_B}(2^{R_0}(1 + \tau) - 1) \quad (58)$$

$$= \frac{m_B^{m_B}}{\Gamma(m_B)} \sum_{j_B=0}^{\infty} \frac{K_B^{j_B} d_{j_B}}{j_B! j_B!} \Upsilon\left(j_B + 1, \frac{2^{R_0}(1 + \tau) - 1}{2\beta_1^2 \sigma_B^2}\right). \quad (59)$$

$$\begin{aligned}\mathcal{I}_1 &= \frac{m_B^{m_B} m_E^{m_E}}{\ln 2 \Gamma(m_B) \Gamma(m_E)} \sum_{j_B=0}^{\infty} \sum_{j_E=0}^{\infty} \frac{K_B^{j_B} d_{j_B} K_E^{j_E} d_{j_E}}{j_B! j_B! j_E! (2\beta_1^2 \sigma_B^2)^{j_B+1}} \left(\chi - \sum_{n=0}^{j_E} \frac{1}{n! (2\mu \sigma_E^2)^n} \Psi(1, j_B + n, n, \frac{1}{2\beta_1^2 \sigma_B^2}, \frac{1}{2\mu \sigma_E^2}, \tau)\right) \\ &\quad + \frac{m_B^{m_B}}{\ln 2 \Gamma(m_B)} \sum_{j_B=0}^{\infty} \frac{K_B^{j_B} d_{j_B}}{j_B! j_B! (2\beta_1^2 \sigma_B^2)^{j_B+1}} \left(S(j_B + 1, \frac{1}{2\beta_1^2 \sigma_B^2}) - \chi\right)\end{aligned}\quad (48)$$

$$\begin{aligned}\mathcal{I}_2 &= \frac{m_B^{m_B} m_E^{m_E}}{\ln 2 \Gamma(m_B) \Gamma(m_E)} \sum_{j_B=0}^{\infty} \sum_{j_E=0}^{\infty} \frac{K_B^{j_B} d_{j_B} K_E^{j_E} d_{j_E} \tau}{j_B! j_E! j_E! (2\mu \sigma_E^2)^{j_E+1}} \\ &\quad \cdot \left(\Psi(1, j_E, j_E + 2, 0, \frac{1}{2\mu \sigma_E^2}, \tau) - \sum_{n=0}^{j_B} \frac{1}{n! (2\beta_1^2 \sigma_B^2)^n} \Psi(1, j_E + n, j_E + 2, \frac{1}{2\beta_1^2 \sigma_B^2}, \frac{1}{2\mu \sigma_E^2}, \tau)\right)\end{aligned}\quad (49)$$

TABLE II
SIMULATION PARAMETERS

Parameter	Value
Central frequency, f_0	30 GHz
Fixed frequency increment, Δf	20 kHz
Number of FDA elements, $2N + 1$	21
Number of subcarriers for each element, L	7
Total signal power, P_s	1
Power splitting factor, β_1	0.9, 0.7
AWGN variance, δ_B^2, δ_E^2	1
FTR parameters, (m_B, K_B, Δ_B)	(2.3, 10, 0.5)
FTR parameters, (m_E, K_E, Δ_E)	(5.3, 15, 0.35)
Location of Bob, (r_B, θ_B, ψ_B)	(1 km, 20° , 30°)
Location of Eve, (r_E, θ_E, ψ_E)	(1.5 km, -20° , 25°)
Number of Monte Carlo experiments	10^5
Modulation mode	PSK, QAM

V. NUMERICAL RESULTS

In this section, Monte Carlo experiments are conducted to verify the theoretical analysis, where the ZF method [10], [12], [15], [18]-[23], the SVD method [16], and the NoAN method [29]-[31] are included. The detailed simulation parameters are listed in Table II.

A. Bit Error Rate

Fig. 6 describes the BER performances with $\beta_1 = 0.9$ versus range, azimuth angle, and elevation angle, respectively, where QPSK modulation and SNR = 10 dB are adopted. It can be clearly observed from Fig. 6 that only the receiver along the desired range, azimuth angle and elevation angle can achieve good BER performance, while the receivers at other locations cannot receive the confidential signal. In addition, compared with conventional FDA models [6]-[17], Fig. 6(c) also verifies that an extra dimension, i.e., elevation angle, is realized via the analytical model as analyzed in Section II.

Fig. 7 and Fig. 8 show the BER performances versus SNR (dB) with PSK and QAM modulations, respectively. It is observed that the proposed SP method can achieve almost the same BER performance as the conventional ZF and SVD methods. In addition, Bob exhibits a better BER performance while Eve's BER is much worse, which verifies the physical-layer security of the proposed FDA-DM model. Moreover, the BER of Bob becomes better with larger β_1 , which is because a larger β_1 allocates more power to the useful signal.

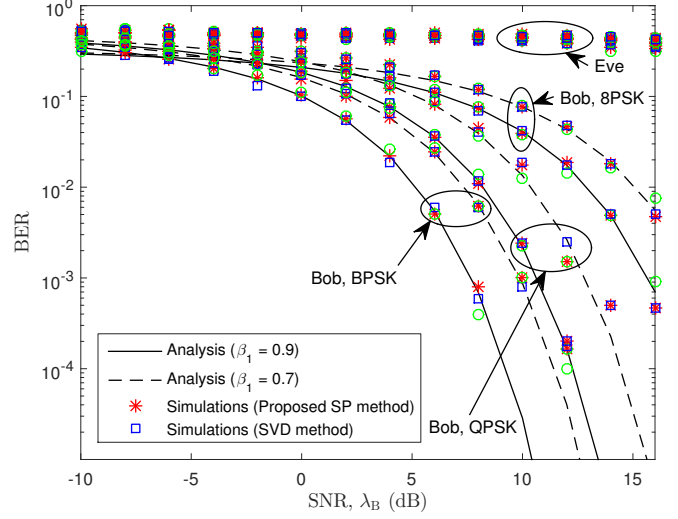


Fig. 7. BER versus SNR (dB) with M -PSK modulations. ($M = 2, 4, 8$, $f_0 = 30$ GHz, $\Delta f = 20$ kHz, $N = 10$, $L = 7$)

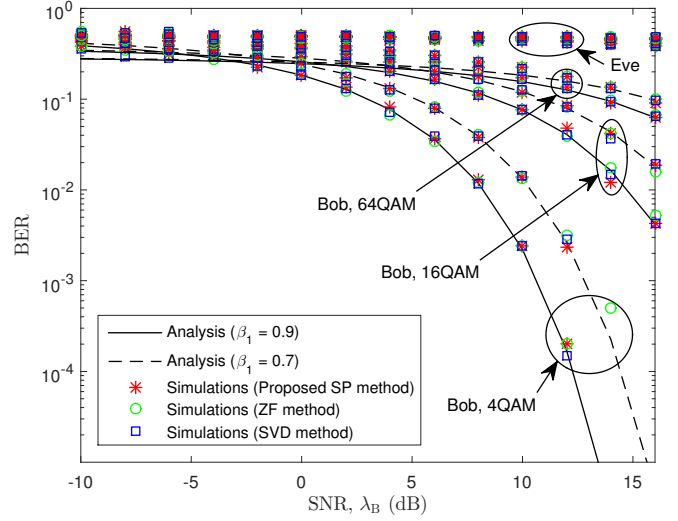


Fig. 8. BER versus SNR (dB) with M -QAM modulations. ($M = 4, 16, 64$, $f_0 = 30$ GHz, $\Delta f = 20$ kHz, $N = 10$, $L = 7$)

$$\mathcal{I}_3 = \frac{m_E^{m_E}}{\ln 2\Gamma(m_E)} \sum_{j_E=0}^{\infty} \frac{K_E^{j_E} d_{j_E} \tau}{j_E! j_E! (2\mu\sigma_E^2)^{j_E+1}} \Psi(1, j_E, j_E + 2, 0, \frac{1}{2\mu\sigma_E^2}, \tau) \quad (50)$$

$$P_{\text{out}} = \frac{m_B^{m_B}}{\Gamma(m_B)} \frac{m_E^{m_E}}{\Gamma(m_E)} \sum_{j_B=0}^{\infty} \sum_{j_E=0}^{\infty} \frac{K_B^{j_B} d_{j_B} K_E^{j_E} d_{j_E} \tau}{j_B! j_E! j_E! (2\mu\sigma_E^2)^{j_E+1}} \left[\Psi(0, j_E, j_E + 2, 0, \frac{1}{2\mu\sigma_E^2}, \tau) \right. \\ \left. - \sum_{n=0}^{j_B} \frac{1}{n!} \exp\left(-\frac{2R_0 - 1}{2\beta_1^2 \sigma_B^2}\right) \sum_{k=0}^n \binom{n}{k} \frac{2^{kR_0} (2R_0 - 1)^{n-k}}{(2\beta_1^2 \sigma_B^2)^n} \Psi(0, j_E + k, j_E + 2, \frac{2R_0}{2\beta_1^2 \sigma_B^2}, \frac{1}{2\mu\sigma_E^2}, \tau) \right] \quad (55)$$

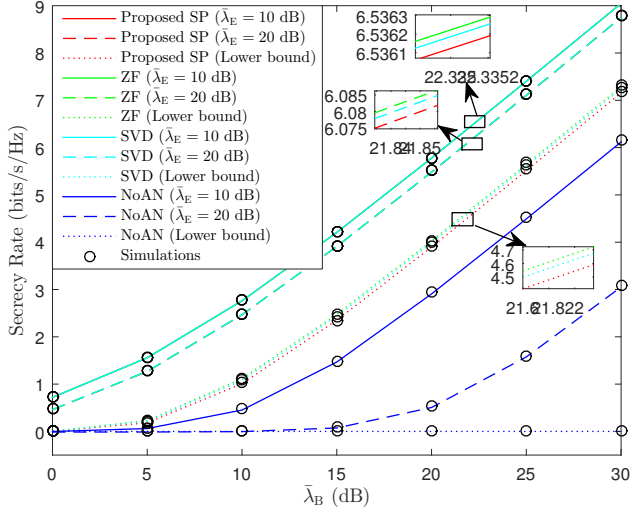


Fig. 9. Average secrecy rate \bar{R}_s versus Bob's average SNR $\bar{\lambda}_B$ (dB) in FTR fading channels. ($f_0 = 30$ GHz, $\Delta f = 20$ kHz, $N = 10$, $L = 7$, $\beta_1 = 0.9$)

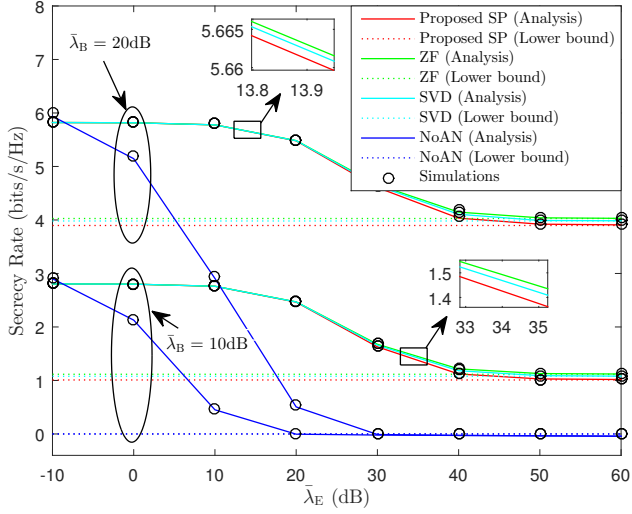


Fig. 10. Average secrecy rate \bar{R}_s versus Eve's average SNR $\bar{\lambda}_E$ (dB) in FTR fading channels. ($f_0 = 30$ GHz, $\Delta f = 20$ kHz, $N = 10$, $L = 7$, $\beta_1 = 0.9$)

B. Secrecy Rate

In the simulations of the average SR, $\beta_1 = 0.9$ is adopted. Fig. 9 depicts the average SR of the proposed FDA-DM scheme versus $\bar{\lambda}_B$ in FTR fading channels, where the analytical results well match the simulated results with 10^5 Monte Carlo experiments. First, it holds for all four PLS approaches that the average SR climbs with increasing $\bar{\lambda}_B$ when $\bar{\lambda}_E$ is fixed. Second, compared with ZF and SVD approaches, the proposed SP method can achieve almost the same average SR. Although there is actually a very small penalty on average SR, the proposed SP method is still much more competitive considering the considerable memory reduction. Moreover, compared with the NoAN approach, there is a positive lower bound for the average SR when $\bar{\lambda}_E \rightarrow \infty$, which means an absolutely positive average SR can always be realized as long as $\bar{\lambda}_B$ is big enough. By contrast, the average SR of NoAN approach reduces to zero when $\bar{\lambda}_E \rightarrow \infty$.

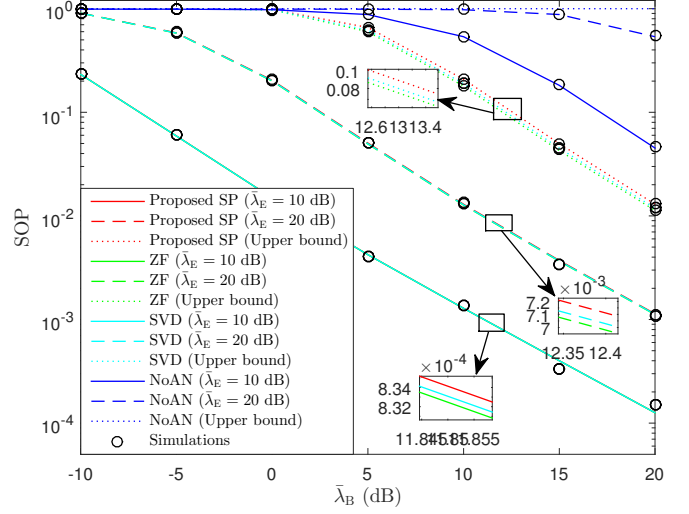


Fig. 11. SOP versus Bob's average SNR $\bar{\lambda}_B$ (dB) with $R_0 = 0$ in FTR fading channels. ($f_0 = 30$ GHz, $\Delta f = 20$ kHz, $N = 10$, $L = 7$, $\beta_1 = 0.9$)

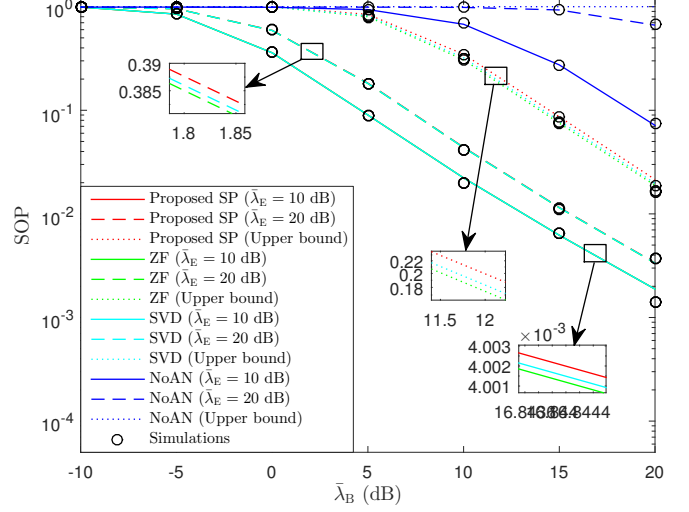


Fig. 12. SOP versus Bob's average SNR $\bar{\lambda}_B$ (dB) with $R_0 = 0.5$ bits/s/Hz in FTR fading channels. ($f_0 = 30$ GHz, $\Delta f = 20$ kHz, $N = 10$, $L = 7$, $\beta_1 = 0.9$)

Fig. 10 illustrates the average SR of the proposed FDA-DM scheme versus $\bar{\lambda}_E$ in FTR fading channels. As expected, that the average SR decreases with increasing $\bar{\lambda}_E$ when $\bar{\lambda}_B$ is fixed. Differently, the average SRs of the proposed SP and the conventional ZF and SVD methods reduce to a positive lower bound, while the average SR of the NoAN method declines to zero. Similar to Fig. 9, almost the same average SR can be achieved for the proposed SP and the conventional ZF and SVD methods while the proposed SP distinguishes from the conventional ZF and SVD methods with much lower memory consumption as analyzed in Section III.A.

C. Secrecy Outage Probability

$\beta_1 = 0.9$ is adopted in the simulations of the SOP as well. Fig. 11 and Fig. 12 present the SOP of the proposed FDA-DM scheme versus $\bar{\lambda}_B$ in FTR fading channels with $R_0 = 0$ and $R_0 = 0.5$ bits/s/Hz, respectively. Comparing Fig. 11 and Fig.

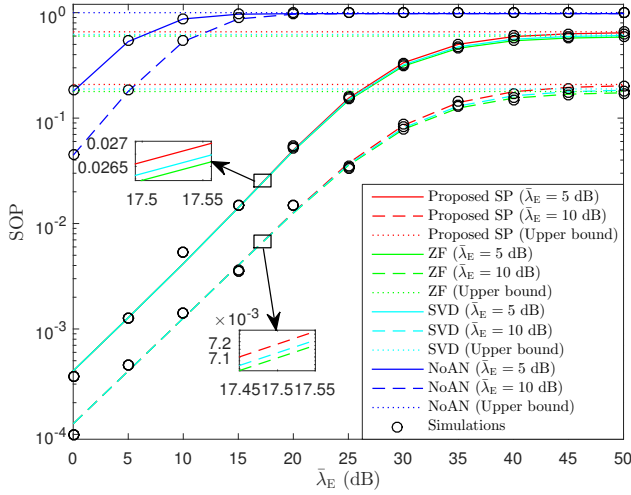


Fig. 13. SOP versus Eve's average SNR $\bar{\lambda}_E$ (dB) with $R_0 = 0$ in FTR fading channels. ($f_0 = 30$ GHz, $\Delta f = 20$ kHz, $N = 10$, $L = 7$, $\beta_1 = 0.9$)

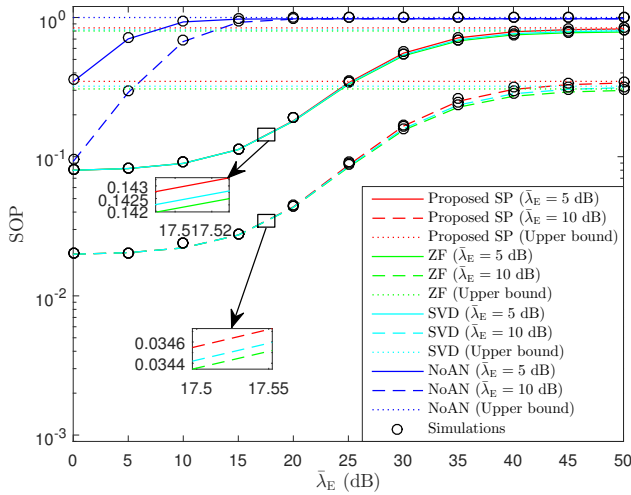


Fig. 14. SOP versus Eve's average SNR $\bar{\lambda}_E$ (dB) with $R_0 = 0.5$ bits/s/Hz in FTR fading channels. ($f_0 = 30$ GHz, $\Delta f = 20$ kHz, $N = 10$, $L = 7$, $\beta_1 = 0.9$)

12, it holds for all four PLS methods that the SOP decreases with smaller R_0 . Given a specific R_0 and $\bar{\lambda}_E$, as expected, the SOP drops as $\bar{\lambda}_B$ increases. Compared with the conventional NoAN method, the proposed SP method can achieve much lower SOP. More importantly, there exists an upper bound of SOP when $\bar{\lambda}_E \rightarrow \infty$ for the proposed SP method, while the SOP of the conventional NoAN method roars to 1. On the other hand, the proposed SP method can achieve almost the same SOP as the conventional ZF and SVD approaches with much lower memory consumption.

Fig. 13 and Fig. 14 illustrate the SOP of the proposed FDA-DM scheme versus $\bar{\lambda}_E$ in FTR fading channels with $R_0 = 0$ and $R_0 = 0.5$ bits/s/Hz, respectively. Analogous to Fig. 11 and Fig. 12, it can also be observed that a smaller R_0 produces a smaller SOP. With a specific R_0 , the SOPs of the proposed SP method and the conventional ZF and SVD methods increase to an upper bound along with increasing $\bar{\lambda}_E$. But for the conventional NoAN method, it roars rapidly to 1

when $\bar{\lambda}_E$ increases. The advantage of the proposed SP method is verified again that much lower memory consumption yet achieves almost the same SOP as the ZF and SVD methods.

VI. CONCLUSION

In this paper, we presented a low-memory-consumption single-point AN-aided secure DM transmission scheme for 5G and beyond communications based on symmetrical multi-carrier FDA, which significantly outperforms the conventional ZF and SVD approaches with only a very small penalty on secrecy rate and secrecy outage probability. In the proposed FDA-DM scheme, the FDA was analyzed in three dimensions, i.e., range, azimuth angle, and elevation angle. Moreover, the secrecy rate and secrecy outage probability of the proposed FDA-DM scheme were analyzed, for the first time, in FTR fading channels, which provide a better fit for small-scale fading measurements in mmWave communications. The closed-form expressions of lower SR bound and upper SOP bound were derived and numerical demonstrations by Monte Carlo experiments were provided as well. One future work is to investigate the PLS performance of the proposed low-memory-consumption FDA-DM scheme with multiple legitimate users.

APPENDIX

A. Proof of Lemma 1

Here, we derive the expression of \mathcal{I}_1 . Substituting (33) and (38) into (42), we can obtain (60)-(62), where $\Upsilon\left(j_E + 1, \frac{\gamma_B}{2\sigma_E^2(\eta - \mu\gamma_B)}\right)$ can be written as [39, Eq. (8.354.1)]

$$\Upsilon\left(j_E + 1, \frac{\gamma_B}{2\sigma_E^2(\eta - \mu\gamma_B)}\right) = j_E! \left(1 - \exp\left(-\frac{\gamma_B}{2\sigma_E^2(\eta - \mu\gamma_B)}\right)\right) \sum_{n=0}^{j_E} \frac{1}{n!} \left(\frac{\gamma_B}{2\sigma_E^2(\eta - \mu\gamma_B)}\right)^n \quad (63)$$

Substituting (63) into (61) and using (43), we can acquire

$$\mathcal{I}_{1,1} = j_E! \Psi\left(1, j_B, 0, \frac{1}{2\beta_1^2 \sigma_B^2}, 0, \tau\right) - j_E! \sum_{n=0}^{j_E} \frac{1}{n! (2\mu\sigma_E^2)^n} \Psi\left(1, j_B + n, n, \frac{1}{2\beta_1^2 \sigma_B^2}, \frac{1}{2\mu\sigma_E^2}, \tau\right) \quad (64)$$

Similarly, $\mathcal{I}_{1,2}$ can be calculated by

$$\mathcal{I}_{1,2} = \Psi\left(1, j_B, 0, \frac{1}{2\beta_1^2 \sigma_B^2}, 0, \infty\right) - \Psi\left(1, j_B, 0, \frac{1}{2\beta_1^2 \sigma_B^2}, 0, \tau\right) \quad (65)$$

Substituting (64) and (65) into (61) and (62), we can get the expression of \mathcal{I}_1 in (48). \mathcal{I}_2 and \mathcal{I}_3 can be derived in the same way, which ends the proof of Lemma 1.

B. Proof of Lemma 2

Observing (29), when $\sigma_E^2 \rightarrow \infty$, we can subsequently obtain $\lambda_E \rightarrow \infty$ and $\gamma_E \rightarrow \tau$. Therefore, \bar{R}_s^{Low} can be written as

$$\begin{aligned}\bar{R}_s^{\text{Low}}(\gamma_B, \gamma_E) &= \frac{1}{\ln 2} \int_0^\infty [\ln(1 + \gamma_B) - \ln(1 + \tau)]^+ f_{\gamma_B}(\gamma_B) d\gamma_B \\ &= \frac{1}{\ln 2} \int_\tau^\infty \ln(1 + \gamma_B) f_{\gamma_B}(\gamma_B) d\gamma_B \\ &\quad - \frac{1}{\ln 2} \int_\tau^\infty \ln(1 + \tau) f_{\gamma_B}(\gamma_B) d\gamma_B\end{aligned}\quad (66)$$

Replacing (30) and (33) into (66) yields (67) and (68), and substituting (43) into (68) ends the proof of Lemma 2.

C. Proof of Lemma 3

Given a fixed secrecy rate R_0 , the SOP in (54) can be further written as

$$P_{\text{out}} = \Pr \{ \gamma_B < 2^{R_0}(1 + \gamma_E) - 1 \} \quad (69)$$

$$= \int_0^\infty F_{\gamma_B}(2^{R_0}(1 + \gamma_E) - 1) f_{\gamma_E}(\gamma_E) d\gamma_E \quad (70)$$

Then, replacing (30), (33) and (40) into (70) yields (71)-(73). Using [39, Eq. (8.354.1)], (73) can be calculated by (74)-(77). According to the binomial theorem [39, Eq. (1.111)], we can write

$$\begin{aligned}\left(\frac{2^{R_0}(1 + \gamma_E) - 1}{2\beta_1^2\sigma_B^2} \right)^n &= \left(\frac{2^{R_0}}{2\beta_1^2\sigma_B^2} \gamma_E + \frac{2^{R_0} - 1}{2\beta_1^2\sigma_B^2} \right)^n \\ &= \frac{2^{nR_0}}{(2\beta_1^2\sigma_B^2)^n} \sum_{k=0}^n \binom{n}{k} \gamma_E^k \left(\frac{2^{R_0} - 1}{2^{R_0}} \right)^{n-k}\end{aligned}\quad (78)$$

Therefore, \mathcal{B} can be acquired in (80)-(82) by replacing (79) into (76). Finally, substituting (77) and (82) into (73) ends the proof of Lemma 3.

ACKNOWLEDGMENT

The authors would like to thank Dr. Jiakang Zheng and Prof. Jiayi Zhang who provided constructive suggestions about the theoretical PDF calculation of FTR fading channels.

REFERENCES

- [1] Y. Wu, A. Khisti, C. Xiao, G. Caire, K.-K. Wong, and X. Gao, "A survey of physical layer security techniques for 5G wireless networks and challenges ahead," *IEEE J. Sel. Areas Commun.*, vol. 36, no. 4, pp. 679-695, Apr. 2018.
- [2] Y. Ding and V. Fusco, "A review of directional modulation technology," *Int. J. Microw. Wirel. Tech.*, vol. 8, no. 7, pp. 981-993, Nov. 2016.
- [3] W.-Q. Wang and Z. Zheng, "Hybrid MIMO and phased-array directional modulation for physical layer security in mmWave wireless communications," *IEEE J. Sel. Areas Commun.*, vol. 36, no. 7, pp. 1383-1396, Jul. 2018.
- [4] S. Y. Nusenu, "Development of frequency modulated array antennas for millimeter-wave communications," *Wirel. Commun. & Mobile Computing*, vol. 2019, pp. 1-16, Apr. 2019.
- [5] M. P. Daly and J. T. Bernhard, "Directional modulation technique for phased arrays," *IEEE Trans. Ant. & Propag.*, vol. 57, no. 9, pp. 2633-2640, Sep. 2009.
- [6] W.-Q. Wang, "Frequency diverse array antenna: new opportunities," *IEEE Ant. & Propag. Magaz.*, vol. 57, no. 2, pp. 145-152, Apr. 2015.
- [7] S. Y. Nusenu and A. Basit, "Frequency diverse array antennas: from their origin to their application in wireless communication systems," *J. Computer Netw. & Commun.*, vol. 2018, pp. 1-12, May 2018.
- [8] J. Xiong, S. Y. Nusenu, and W.-Q. Wang, "Directional modulation using frequency diverse array for secure communications," *Wirel. Personal Commun.*, vol. 95, no. 3, pp. 2679-2689, Aug. 2017.
- [9] W.-Q. Wang, "DM using FDA antenna for secure transmission," *IET Microw. Ant. & Propag.*, vol. 11, no. 3, pp. 336-345, Apr. 2017.
- [10] J. Hu, S. Yan, F. Shu, J. Wang, J. Li, and Y. Zhang, "Artificial-noise-aided secure transmission with directional modulation based on random frequency diverse arrays," *IEEE Access*, vol. 5, no. 99, pp. 1658-1667, Jan. 2017.
- [11] Q. Cheng, J. Zhu, T. Xie, J. Luo, and Z. Xu, "Time-invariant angle-range dependent directional modulation based on time-modulated frequency diverse arrays," *IEEE Access*, vol. 5, pp. 26279-26290, Dec. 2017.
- [12] B. Qiu, J. Xie, L. Wang, and Y. Wang, "Artificial-noise-aided secure transmission for proximal legitimate user and eavesdropper based on frequency diverse arrays," *IEEE Access*, vol. 6, pp. 52531-52543, 2018.
- [13] J. Lin, Q. Li, J. Yang, H. Shao, and W.-Q. Wang, "Physical-layer security for proximal legitimate user and eavesdropper: a frequency diverse array beamforming approach," *IEEE Trans. Inform. Forens. & Sec.*, vol. 13, no. 3, pp. 671-684, Mar. 2018.

$$\mathcal{I}_1 = \frac{1}{\ln 2} \int_0^\tau \ln(1 + \gamma_B) f_{\gamma_B}(\gamma_B) F_{\gamma_E}(\gamma_B) d\gamma_B + \frac{1}{\ln 2} \int_\tau^\infty \ln(1 + \gamma_B) f_{\gamma_B}(\gamma_B) F_{\gamma_E}(\gamma_B) d\gamma_B \quad (60)$$

$$= \frac{m_B^{m_B} m_E^{m_E}}{\ln 2 \Gamma(m_B) \Gamma(m_E)} \sum_{j_B=0}^\infty \sum_{j_E=0}^\infty \frac{K_B^{j_B} d_{j_B} K_E^{j_E} d_{j_E}}{j_B! j_B! j_E! j_E! (2\beta_1^2 \sigma_B^2)^{j_B+1}} \underbrace{\int_0^\tau \ln(1 + \gamma_B) \gamma_B^{j_B} \exp\left(-\frac{\gamma_B}{2\beta_1^2 \sigma_B^2}\right) \Upsilon\left(j_E + 1, \frac{\gamma_B}{2\sigma_E^2(\eta - \mu\gamma_B)}\right) d\gamma_B}_{\mathcal{I}_{1,1}} \quad (61)$$

$$+ \frac{m_B^{m_B}}{\ln 2 \Gamma(m_B)} \sum_{j_B=0}^\infty \frac{K_B^{j_B} d_{j_B}}{j_B! j_B! (2\beta_1^2 \sigma_B^2)^{j_B+1}} \underbrace{\int_\tau^\infty \ln(1 + \gamma_B) \gamma_B^{j_B} \exp\left(-\frac{\gamma_B}{2\beta_1^2 \sigma_B^2}\right) d\gamma_B}_{\mathcal{I}_{1,2}} \quad (62)$$

$$\bar{R}_s^{\text{Low}}(\gamma_B, \gamma_E) = \frac{1}{\ln 2} \int_\tau^\infty \ln(1 + \gamma_B) \frac{m_B^{m_B}}{\Gamma(m_B)} \sum_{j_B=0}^\infty \frac{K_B^{j_B} d_{j_B}}{j_B! j_B!} \frac{\gamma_B^{j_B}}{(2\beta_1^2 \sigma_B^2)^{j_B+1}} \exp\left(-\frac{\gamma_B}{2\beta_1^2 \sigma_B^2}\right) d\gamma_B - \frac{\ln(1 + \tau)}{\ln 2} [1 - F_{\gamma_B}(\tau)] \quad (67)$$

$$= \frac{m_B^{m_B}}{\ln 2 \Gamma(m_B)} \sum_{j_B=0}^\infty \frac{K_B^{j_B} d_{j_B}}{j_B! j_B! (2\beta_1^2 \sigma_B^2)^{j_B+1}} \int_\tau^\infty \ln(1 + \gamma_B) \gamma_B^{j_B} \exp\left(-\frac{\gamma_B}{2\beta_1^2 \sigma_B^2}\right) d\gamma_B - \frac{\ln(1 + \tau)}{\ln 2} [1 - F_{\gamma_B}(\tau)] \quad (68)$$

- [14] T. Xie, J. Zhu, Q. Cheng, and Y. Guan, "Secure point-to-multipoint communication using the spread spectrum assisted orthogonal frequency diverse array in free space," *IEICE Trans. Commun.*, vol. E102.B, no. 6, pp. 1188-1197, Jun. 2019.
- [15] B. Qiu, M. Tao, L. Wang, J. Xie, and Y. Wang, "Multi-beam directional modulation synthesis scheme based on frequency diverse array," *IEEE Trans. Info. Foren. & Sec.*, vol. 14, no. 10, pp. 2593-2606, Oct. 2019.
- [16] Q. Cheng, V. Fusco, J. Zhu, S. Wang, and C. Gu, "SVD-aided multi-beam directional modulation scheme based on frequency diverse array," *arXiv: 1907.11972v1*, Jul. 2019.
- [17] Q. Cheng, V. Fusco, J. Zhu, S. Wang, and F. Wang, "WFRFT-aided power-efficient multi-beam directional modulation schemes based on frequency diverse array," Accepted by *IEEE Trans. Wirel. Commun.*, to appear, DOI: 10.1109/TWC.2019.2934462.
- [18] J. Hu, F. Shu, and J. Li, "Robust synthesis method for secure directional modulation with imperfect direction angle," *IEEE Commun. Lett.*, vol. 20, no. 6, pp. 1084-1087, Jun. 2016.
- [19] F. Shu, L. Xu, J. Wang, W. Zhu, and X. Zhou, "Artificial-noise-aided secure multicast precoding for directional modulation systems," *IEEE Trans. Veh. Tech.*, vol. 67, no. 7, pp. 6658-6662, Jul. 2018.
- [20] T. Xie, J. Zhu, and Y. Li, "Artificial-noise-aided zero-forcing synthesis approach for secure multi-beam directional modulation," *IEEE Commun. Lett.*, vol. 22, no. 2, pp. 276-279, Feb. 2018.
- [21] S. Ji, W.-Q. Wang, H. Chen, and S. Zhang, "On physical-layer security of FDA communications over Rayleigh fading channels," Accepted by *IEEE Trans. Cogn. Commun. and Net.*, to appear, DOI: 10.1109/TCCN.2019.2906896.
- [22] S. Ji, W.-Q. Wang, H. Chen, and Z. Zheng, "Secrecy capacity analysis of AN-aided FDA communication over Nakagami- m fading," *IEEE Wirel. Commun. Lett.*, vol. 7, no. 6, pp. 1034-1037, Dec. 2018.
- [23] S. Ji and W.-Q. Wang, "Physical-layer security for frequency diverse array communication system over Nakagami- m fading channels," Accepted by *IEEE Systems Journal*, to appear, DOI: 10.1109/JSYST.2019.2923103.
- [24] J. M. Romero-Jerez, F. J. Lopez-Martinez, J. F. Paris, and A. J. Goldsmith, "The fluctuating two-ray fading model for mmWave communications," in *Proceedings of 2016 IEEE Globecom Workshops*, Washington, DC, USA, Dec. 2016, pp. 1-6.
- [25] J. M. Romero-Jerez, F. J. Lopez-Martinez, J. F. Paris, and A. J. Goldsmith, "The fluctuating two-ray fading model: Statistical characterization and performance analysis," *IEEE Trans. Wireless Commun.*, vol. 16, no. 7, pp. 4420-4432, Jul. 2017.
- [26] J. Zhang, W. Zeng, X. Li, Q. Sun, and K. P. Peppas, "New results on the fluctuating two-ray model with arbitrary fading parameters and its applications," *IEEE Trans. Veh. Technol.*, vol. 67, no. 3, pp. 2766-2770, Mar. 2018.
- [27] O. S. Badarneh and D. B. da Costa, "Cascaded fluctuating two-ray fading channel," Accepted by *IEEE Commun. Lett.*, to appear, DOI: 10.1109/LCOMM.2019.2926982.
- [28] J. Zheng, J. Zhang, G. Pan, J. Cheng, and B. Ai, "Sum of squared fluctuating two-ray random variables with wireless applications," *IEEE Trans. Veh. Technol.*, vol. 35, no. 8, pp. 8173-8177, Aug. 2019.
- [29] W. Zeng, J. Zhang, S. Chen, K. P. Peppas, and B. Ai, "Physical layer security over fluctuating two-ray fading channels," *IEEE Trans. Veh. Technol.*, vol. 67, no. 9, pp. 8949-8953, Sept. 2018.
- [30] H. Zhao, L. Yang, G. Pan, and M.-S. Alouimi, "Secrecy outage analysis over fluctuating two-ray fading channels," *Arxiv: 1905.12396v1*, May 2019.
- [31] M. Bilim and N. Kapucu, "Average symbol error rate analysis of QAM schemes over millimeter wave fluctuating two-ray fading channels," *IEEE Access*, vol. 7, pp. 105746-105754, Aug. 2019.
- [32] H. Zhao, Z. Liu, and M.-S. Alouimi, "Different power adaption methods on fluctuating two-ray fading channels," *IEEE Wirel. Commun. Lett.*, vol. 8, no. 2, pp. 592-595, Apr. 2019.
- [33] J. Zheng, J. Zhang, S. Chen, H. Zhao, and B. Ai, "Wireless powered UAV relay communications over fluctuating two-ray fading channels," *Physical Commun.*, vol. 35, pp. 1-8, May 2019.
- [34] H. Shao, J. Dai, J. Xiong, H. Chen, and W.-Q. Wang, "Dot-shaped range-angle beampattern synthesis for frequency diverse array," *IEEE Ante. & Wirel. Propag. Lett.*, vol. 15, pp. 1703-1706, Feb. 2016.
- [35] Y. Ding and V. Fusco, "Establishing metrics for assessing the performance of directional modulation systems," *IEEE Trans. Ante. & Propag.*, vol. 62, no. 5, pp. 2745-2755, May 2014.
- [36] H. Yomo and E. D. Carvalho, "A CSI estimation method for wireless

$$P_{\text{out}} = \int_0^\tau \frac{m_B^{m_B}}{\Gamma(m_B)} \sum_{j_B=0}^{\infty} \frac{K_B^{j_B} d_{j_B}}{j_B! j_B!} \Upsilon \left(j_B + 1, \frac{2^{R_0}(1 + \gamma_E) - 1}{2\beta_1^2 \sigma_B^2} \right) \frac{\eta}{(\eta - \mu\gamma_E)^2} \frac{m_E^{m_E}}{\Gamma(m_E)} \sum_{j_E=0}^{\infty} \frac{K_E^{j_E} d_{j_E}}{j_E! j_E!} \frac{(\frac{\gamma_E}{\eta - \mu\gamma_E})^{j_E}}{(2\sigma_E^2)^{j_E+1}} \exp \left(-\frac{\gamma_E}{2\sigma_E^2} \right) d\gamma_E \quad (71)$$

$$= \frac{m_B^{m_B}}{\Gamma(m_B)} \frac{m_E^{m_E}}{\Gamma(m_E)} \sum_{j_B=0}^{\infty} \sum_{j_E=0}^{\infty} \frac{K_B^{j_B} d_{j_B} K_E^{j_E} d_{j_E} \tau}{j_B! j_B! j_E! j_E! (2\mu\sigma_E^2)^{j_E+1}} \quad (72)$$

$$\cdot \underbrace{\int_0^\tau \Upsilon \left(j_B + 1, \frac{2^{R_0}(1 + \gamma_E) - 1}{2\beta_1^2 \sigma_B^2} \right) \frac{\gamma_E^{j_E}}{(\tau - \gamma_E)^{j_E+2}} \exp \left(-\frac{\gamma_E}{2\mu\sigma_E^2(\tau - \gamma_E)} \right) d\gamma_E}_{\mathcal{A}} \quad (73)$$

$$\mathcal{A} = \int_0^\tau j_B! \left(1 - \exp \left(-\frac{2^{R_0}(1 + \gamma_E) - 1}{2\beta_1^2 \sigma_B^2} \right) \right) \sum_{n=0}^{j_B} \frac{1}{n!} \left(\frac{2^{R_0}(1 + \gamma_E) - 1}{2\beta_1^2 \sigma_B^2} \right)^n \frac{\gamma_E^{j_E}}{(\tau - \gamma_E)^{j_E+2}} \exp \left(-\frac{\gamma_E}{2\mu\sigma_E^2(\tau - \gamma_E)} \right) d\gamma_E \quad (74)$$

$$= j_B! \int_0^\tau \frac{\gamma_E^{j_E}}{(\tau - \gamma_E)^{j_E+2}} \exp \left(-\frac{\gamma_E}{2\mu\sigma_E^2(\tau - \gamma_E)} \right) d\gamma_E \quad (75)$$

$$- \sum_{n=0}^{j_B} \frac{j_B!}{n!} \int_0^\tau \frac{\gamma_E^{j_E}}{(\tau - \gamma_E)^{j_E+2}} \underbrace{\left(\frac{2^{R_0}(1 + \gamma_E) - 1}{2\beta_1^2 \sigma_B^2} \right)^n \exp \left(-\frac{\gamma_E}{2\mu\sigma_E^2(\tau - \gamma_E)} - \frac{2^{R_0}(1 + \gamma_E) - 1}{2\beta_1^2 \sigma_B^2} \right)}_{\mathcal{B}} d\gamma_E \quad (76)$$

$$= j_B! \Psi(0, j_E, j_E + 2, 0, \frac{1}{2\mu\sigma_E^2}, \tau) - \sum_{n=0}^{j_B} \frac{j_B!}{n!} \mathcal{B} \quad (77)$$

relay network,” *IEEE Commun. Lett.*, vol. 11, no. 6, pp. 480-482, Jun. 2007.

- [37] H. Wu, Y. Jia, and S. B. Simmons, “Method and apparatus for LTE channel state information estimation,” U.S. Patent US9294310B2, Mar. 22 2016.
- [38] J. G. Proakis and M. Salehi, “Optimum receivers for AWGN channels,” in *Digital Commun.*, 5th ed., New York, NY, USA: McGraw-Hill, 2007, pp. 190-195.
- [39] I. S. Gradshteyn and I. M. Ryzhik, *Table of Integrals, Series, and Products*, 7th ed. Academic Press, California, 2007.



Qian Cheng received the B.S. degree in Information and Communication Engineering from Xidian University, Xi'an, China, in 2014, and the M.S. degree in Information and Communication Engineering from the National University of Defense Technology (NUDT), Changsha, China, in 2016, where he is currently pursuing the Ph.D. degree.

He is also a Visiting Ph.D. Researcher with the Institute of Electronics, Communications and Information Technology (ECIT), Queen's University Belfast, Belfast, U.K. His research interests include physical layer security and directional modulation.

physical layer security and directional modulation.



Shilian Wang received his B.S. and Ph.D. degrees in information and communication engineering from National University of Defense Technology (NUDT), Changsha, China, in 1998 and 2004, respectively. Since 2004, he continued research in wireless communications at NUDT, where he later became a Professor. From 2008 to 2009, he was a visiting scholar with the Department of Electronic and Electrical Engineering at Columbia University (CU), New York, USA.

He is currently the Head of the Laboratory of Advanced Communication Technology at the School of Electronic Science, NUDT. He has authored or co-authored two books, 26 journal papers, and 20 conference papers. His research interests include wireless communications and signal processing theory, including chaotic spread spectrum and LPI communications, physical layer security, spatial modulation, deep learning and its applications in communication sensing, etc.



Vincent Fusco (S'82-M'82-SM'96-F'04) received the bachelor's degree (Hons.) in electrical and electronic engineering, the Ph.D. degree in microwave electronics, and the D.Sc. degree from Queen's University Belfast (QUB), Belfast, U.K., in 1979, 1982, and 2000, respectively.

He is currently a Chief Technology Officer with the Institute of Electronics, Communications and Information Technology (ECIT), QUB. He has authored more than 450 scientific papers in major journals and in referred international conferences and two textbooks. He holds patents related to self-tracking antennas and has contributed invited papers and book chapters. His current research interests include advanced front-end architectures with enhanced functionality, active antenna, and front-end MMIC techniques.

Dr. Fusco is a Fellow of the Institution of Engineering and Technology, the Royal Academy of Engineers, and the Royal Irish Academy. He was a recipient of the IET Senior Achievement Award and the Mountbatten Medal, in 2012. He serves on the Technical Program Committee of various international conferences, including the European Microwave Conference.



Fanggang Wang (S'10-M'11-SM'16) received the B.Eng. and Ph.D. degrees from the School of Information and Communication Engineering, Beijing University of Posts and Telecommunications, Beijing, China, in 2005 and 2010, respectively. He was a Post-Doctoral Fellow with the Institute of Network Coding, The Chinese University of Hong Kong, Hong Kong, from 2010 to 2012. He was a Visiting Scholar with the Massachusetts Institute of Technology from 2015 to 2016, and with the Singapore University of Technology and Design in 2014.

He is currently a Professor with the State Key Laboratory of Rail Traffic Control and Safety, School of Electronic and Information Engineering, Beijing Jiaotong University. His research interests are in wireless communications, signal processing, and information theory. He served as an Editor for the IEEE Communications Letters and a technical program committee member for several conferences.



Jiang Zhu received the B.S., M.S., and Ph.D. degrees in electrical engineering from the National University of Defense Technology (NUDT), Changsha, China, in 1994, 1997, and 2000, respectively. From 2000 to 2004, he was a lecturer in communication engineering at the NUDT. He was a visiting scholar at the University of Calgary, AB, Canada from April 2004 to July 2005. From 2005 to 2008, he was an associate professor in communication engineering at the NUDT.

Since 2008, he has been with the NUDT as a full professor in the School of Electronic Science and Engineering. His current research interests include wireless high speed communication technology, satellite communication, physical layer security and wireless sensor network.

$$\mathcal{B} = \int_0^\tau \frac{\gamma_E^{j_E}}{(\tau - \gamma_E)^{j_E+2}} \frac{2^{nR_0}}{(2\beta_1^2\sigma_B^2)^n} \sum_{k=0}^n \binom{n}{k} \gamma_E^k \left(\frac{2^{R_0} - 1}{2^{R_0}} \right)^{n-k} \exp \left(-\frac{\gamma_E}{2\mu\sigma_E^2(\tau - \gamma_E)} - \frac{2^{R_0}(1 + \gamma_E) - 1}{2\beta_1^2\sigma_B^2} \right) d\gamma_E \quad (80)$$

$$= \exp \left(-\frac{2^{R_0} - 1}{2\beta_1^2\sigma_B^2} \right) \sum_{k=0}^n \binom{n}{k} \frac{2^{kR_0}(2^{R_0} - 1)^{n-k}}{(2\beta_1^2\sigma_B^2)^n} \int_0^\tau \frac{\gamma_E^{j_E+k}}{(\tau - \gamma_E)^{j_E+2}} \exp \left(-\frac{\gamma_E}{2\mu\sigma_E^2(\tau - \gamma_E)} - \frac{2^{R_0}\gamma_E}{2\beta_1^2\sigma_B^2} \right) d\gamma_E \quad (81)$$

$$= \exp \left(-\frac{2^{R_0} - 1}{2\beta_1^2\sigma_B^2} \right) \sum_{k=0}^n \binom{n}{k} \frac{2^{kR_0}(2^{R_0} - 1)^{n-k}}{(2\beta_1^2\sigma_B^2)^n} \Psi(0, j_E + k, j_E + 2, \frac{2^{R_0}}{2\beta_1^2\sigma_B^2}, \frac{1}{2\mu\sigma_E^2}, \tau) \quad (82)$$



Chao Gu received the B.S. and M.S. degrees in electronic engineering from Xidian University, Xi'an, China, in 2009 and 2012, respectively, and the Ph.D. degree in electronic engineering at University of Kent, Canterbury, U.K., in 2017. He is currently a senior engineer at the ECIT Institute, Queen's University Belfast, Belfast, U.K. His research interests include smart antennas, reconfigurable antennas, and frequency selective surfaces.